NEW MATERIALS FROM MULTISCALE MODELLING PROCEDURES: PROPERTIES PREDICTION AND CUSTOMISATION OF POLYMERIC NANOCOMPOSITES

Paolo Cosoli[a], Giulio Scocchi[a,b], Marco Ferrone[a], Andrea Danani[b], Paola Posocco[a], Maurizio Fermeglia[a] Sabrina Pricl[a],

[a] Molecular Simulation Engineering (MOSE) laboratory, DICAMP, Università degli Studi di Trieste, P.le Europa 1, 34127 Trieste, Italy
[b] Department of Innovative Technologies, SUPSI, Le Gerre, Manno, CH6928, Switzerland

This work describes procedures and potentialities of multiscale molecular modeling for the design of nanostructured materials. These relatively new techniques are now opening unexplored frontiers in the fields of material sciences. Nowadays, nanocomposite materials are growing up in interest, due to their improved characteristics for industrial applications. This is specially the case of nanoengineered polymers, which offer better performances in terms of thermal, mechanical and barrier properties. This paper focuses on polymer-clay nanocomposites and, in particular, on the possibilities of application of *ab initio* and *totally-in-silico* procedures based on multiscale molecular modeling for the calculation of mechanical, thermodynamic and structural properties of these materials. We report two examples of application of our computational recipes based on innovative, step-by-step procedures, in which each calculation at a given level (e.g., atomistic, mesoscale, etc.) yields information necessary to perform simulation at the next, higher length/time scale level.

1. INTRODUCTION

In the last decades molecular simulation techniques have been recognized as a powerful tool to investigate and predict materials morphologies and behavior. Moreover, progressive improvements in CPU performances and new algorithms to overcome the limits of atomistic and quantum-mechanics calculations have now opened new possibilities to couple different length and time scale simulations (Charpentier, 2002). In this way, multiscale procedures allow to study thermodynamic, structural and mechanical properties with *totally-in-silico* procedures.
Today, the interest about polymer-clay nanocomposites (PCNs) is considerably increasing, due to the improved performances they may offer (Utracki, 2004). This work describes two different procedures for the design of a nanocomposite of industrial interest with the exclusive use of multiscale molecular simulation techniques.
Our approach to multiscale simulations is based on the principle that the set of outputs from lower length and/or time scale calculations should be used as input data for higher scale simulations. These procedures allow determining characteristic behaviors, such as: (i) the structure and partial charge of nanocomposite constituents (quantum-mechanics), (ii) the ranking and eventual selection of the best nanocomposite surfactants, which enlarge clay layers and favor polymer penetration and, hence, platelet exfoliation (atomistic level); (iii) the characteristics of the exfoliation/intercalation of the clay platelets (atomistic level), (iv) the morphology of the polymer matrix (atomistic or/and mesoscale level) and (v) the mechanical properties of polymer blends and/or nanocomposite (finite elements simulations).
Figure 1 reports the ranges of application in terms of time and length for the different modules employed in multiscale simulations.

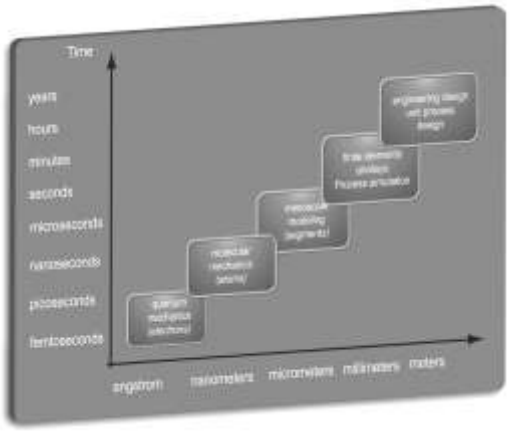

Figure 1: multiscale molecular modeling in terms of time and length for the different modules employed.

In order to show the applicability of the methodology, this paper will present two different procedures applied to two kinds of polymer-clay nanocomposites (Cosoli et al., 2007; Scocchi et al., 2007). One will focus on the ABS-MMT system, which is constituted by a complex polymer blend (acrylonitrile-butadiene-styrene) and by montmorillonite (MMT) clay. ABS is a polymeric blend of industrial interest; its mechanical properties may be greatly enhanced by a small quantity (e.g. 2% w/w) of MMT. The second system presented here is a polyamide6-MMT based nanocomposite; this combination is selected as an ideal reference system, by virtue of the numerous experimental studies available for this PCN in the scientific literature. As for the ABS/MMT system, properties can be enhanced by adding a small quantity of clay. Moreover, exfoliation using polyamide is known to be feasible without major problems. For this PCN, in particular, the following 2 systems were selected to test and validate our computational approach: MMT/Nylon6/trimethyl-dehydrogenated tallow quaternary ammonium chloride, and MMT/Nylon6/dimethyl-dehydrogenated tallow quaternary ammonium chloride, respectively.
In the next paragraph it will be shown how each time-length scale simulation method was used to characterize the exfoliation process, the morphology of blends and nanocomposite, and the relevant mechanical properties. In the results and discussion section experimental validation obtained against literature data will be reported. Both these PCN systems have been selected because they are representative of complex situations, that summarize all the characteristics of typical problems encountered both in polymer blends and in nanocomposite preparation.

2. METHODS

2.1 Quantum-mechanics

Quantum mechanics (QM) methods are used to calculate the partial charges, bond lengths and angles for the surfactant molecules (also called quats) and the polymer repetitive units. Quats 3D model building have been obtained by standard QM methods (Tanaka et al. 2002). These data can be easily imported and used in the next level of length/time scale calculations, i.e., atomistic molecular mechanics and dynamics.

2.2 Molecular mechanics and dynamics

Molecular simulations of quats intercalation between MMT layers, and MMT exfoliation, can be performed by molecular mechanics and dynamics (MM/MD). Such simulations are carried out with the aim of the aim of determining the thermodynamic behavior of the exfoliated ternary system (MMT-quat-polymer) by examining binding energies of the systems.
The ternary system is modeled following the procedure described in our previous work, (Fermeglia et al., 2003) and (Toth et. al., 2004), as a whole system, and as parts, in order to separate and evaluate each significant contributions to binding energies. Moreover, in the case of the ABS based system, due to the blend

complexity, different copolymer position between MMT layers have been taken into account. Binary binding energies (MMT-polymer, MMT-quat, and polymer-quat) in the corresponding ternary system can be defined as follows:

$$E_{pol-MMT-quat} = E_{pol} + E_{MMT} + E_{quat} + E_{MMT-quat} + E_{MMT-pol} + E_{pol-quat} \quad \textbf{(1)}$$

where the first three terms represent the energy of polymer, MMT and quat, respectively, and the last three terms represent the binary binding energies of MMT-polymer, MMT-quat, and polymer-quat, respectively, defined as follows:

$$E_{MMT-pol} = E_{(MMT+pol)} - \left(E_{MMT} + E_{pol}\right) \quad \textbf{(2)}$$

$$E_{MMT-quat} = E_{(MMT+quat)} - \left(E_{MMT} + E_{quat}\right) \quad \textbf{(3)}$$

$$E_{pol-quat} = E_{(pol+quat)} - \left(E_{pol} + E_{quat}\right) \quad \textbf{(4)}$$

By definition, then, negative values for these energies indicate good thermodynamic compatibility between pairs.

Basal spacing of intercalated quats into MMT layers has been evaluated using isochoric-isothermal (NPT) MD simulations of the MMT-quat binary systems under 3D periodic boundary conditions. In this case, whilst the *x* and *y* cell dimensions are kept fixed, constraints on *z* axis (normal to MMT layers) are removed, in order to reach the equilibrium distance between the layers. This simulations campaign provides the useful information on the available space for polymer insertion after MMT modification by a given quat (Figure 2).

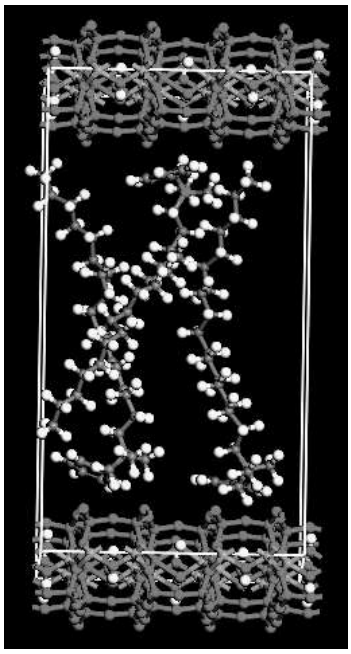

Figure 2: 3D periodic cell of MMT (grey stick-and-ball representation, upper and lower parts of the Figure) and quat (cloisite 10A®, white and grey stick-and-ball representation, central portion of the Figure) employed for basal spacing calculations (reproduced from Cosoli et al. 2007, with permission).

2.3 Mesoscale simulations

Two different mesoscale simulations methods have been applied, namely Mean Field Density Functional Theory (MFDFT), and Dissipative Particle Dynamics (DPD) for the ABS and the polyamide based systems, respectively. The MesoDyn simulation method, based upon the MFDFT (Altevogt et. al., 1999), has been used to predict the phase behavior of the ABS blend. The mesoscale molecular model consists of beads of various types, each one represents a group of monomers in the chains. The size of the bead (e.g., the number of monomers contained in each bead) depends on chain flexibility, and it is related to the polymer characteristic ratio C_∞ which, in turn, can be obtained by performing MD simulations on polymer chains under 3D periodic boundary conditions. The method mainly relies upon the determination of the Flory-Huggins parameters χ_{ij} estimated from the corresponding solubility parameters δ_{ij} which, in turn, are obtained via atomistic MD simulations (Flory, 1974).
Simulations results are given in terms of bead local densities. Accordingly, an order parameters P_I for each bead species I, is introduced as the deviation from the mean bead density at homogeneity (Fermeglia et al. 2006):

$$P_I = \frac{1}{V}\int_V \left[\theta_I^2(r) - \theta_{I,0}^2\right] dr \qquad \textbf{(5)}$$

where θ_I is a dimensionless density for bead species I, and the index 0 denotes average values at homogeneity. Order parameters with large values indicate strong phase segregation. Conversely, very small values of P_I correspond to homogeneous systems.
The DPD simulation method (Hoogerbruge and Koelman, 1992; Koelman and Hoogerbruge, 1993) relies on a completely different approach. A set of particles is set to move according to Newton's equation of motion, and to interact dissipatively through simplified force laws. If the mass of all particles is set to equal to unity, the time evolution of the positions ($\mathbf{r}_i(t)$) and momenta ($\mathbf{p}_i(t)$) is given by the well-known relationships:

$$\frac{d\mathbf{r}_i}{dt} = \mathbf{v}_i(t) \quad \frac{d\mathbf{v}_i}{dt} = \mathbf{f}_i(t) \qquad \textbf{(6)}$$

where $\mathbf{r}_i$, $\mathbf{v}_i$, and $\mathbf{f}_i$ are the position vector, velocity, and total force, respectively, acting on particle i.
The force acting on the particles, which is pairwise additive, can be decomposed into three elements: a conservative ($\mathbf{F}_{ij}^C$), a dissipative ($\mathbf{F}_{ij}^D$), and a random ($\mathbf{F}_{ij}^R$) force. Accordingly, the effective force $\mathbf{f}_i$ acting on a particle i is given by:

$$\mathbf{f}_i = \sum_{i \neq j} \left(\mathbf{F}_{ij}^C + \mathbf{F}_{ij}^D + \mathbf{F}_{ij}^R\right) \qquad \textbf{(7)}$$

where the sum extends over all particles within a given distance r_c from the ith particle. This distance practically constitutes the only length scale in the entire system. Therefore, it is convenient to set the cutoff radius r_c as a unit of length (i.e., $r_c = 1$), so that all lengths are measured relative to the particles radius.
The conservative force is a soft repulsion, given by:

$$\mathbf{F}_{ij}^C = \begin{cases} a_{ij}\left(1 - r_{ij}\right)\hat{\mathbf{r}}_{ij} & \left(r_{ij} < 1\right) \\ 0 & \left(r_{ij} \geq 1\right) \end{cases} \qquad \textbf{(8)}$$

where a_{ij} is the maximum repulsion between particles i and j, r_{ij} is the magnitude of the particle-particle vector $\mathbf{r}_{ij} = \mathbf{r}_i - \mathbf{r}_j$ (i.e., $r_{ij} = |\mathbf{r}_{ij}|$), and $\hat{\mathbf{r}}_{ij} = \mathbf{r}_{ij} / r_{ij}$ is the unit vector joining particles i and j. The other two forces,

$\mathbf{F}_{ij}^{D}$ and $\mathbf{F}_{ij}^{R}$, are both responsible for the conservation of the total momentum in the system, and incorporate the Brownian motion into the larger length scale.
In the DPD model, individual atoms or molecules are not represented directly by the particle, but they are coarse-grained into beads. These beads represent local "fluid packages" able to move independently. Incorporation of chain molecules simply requires the addition of a harmonic spring force between the beads; by means of this spring, the beads can interconnect to highly complex topologies.

2.4 Finite element simulations

Finite element simulations methods (FEM) for polymer blends assume density distributions from mesoscale calculation and, thus, have been used to find PCNs mechanical (e.g., Young's modulus) and barrier properties. FEM programs such as MesoProp and Palmyra (Gusev, 1997), make use of mechanical properties of pure systems, which are available from a database, or calculated with previous simulations. For the ABS-MMT system, Young's modulus, Poisson's ratio and density values have been estimated with the Synthia modulus of Materials Studio (Accelrys, San Diego, USA), which uses linear regression of a set of experimental data available from a database to calculate polymer properties for atomistic models (Bicerano, 2002). For the other PCN considered, mechanical and barrier properties of components have been retrieved from literature.

3. RESULTS AND DISCUSSION

ABS based system. Atomistic simulations allowed us to rank different quats for the selected clay/polymer system. Figure 2 shows a 3D periodic cell for ternary simulations of the ABS-based PCN, while Table 1 lists the binding energies for the best quat resulting from the screening, which is the quaternary, double-tailed ammonium salt Cloisite 20A®, and the relevant spacing between the clay platelets. ABS is a complex system, being constituted by an acrylonitrile (AN)-styrene (S) block copolymer (SAN) and a branched copolymer (polyB-SAN) with a main butadiene (B) chain and lateral chains of SAN. Accordingly, in Table 1 the SAN copolymer is oriented with the S block next to MMT surface and the ANS polymer is the same macromolecule but oriented with AN block next to MMT surface. Similarly, polyB-SAN presents the main chain of B oriented parallel to MMT surface, while polyB-SAN is rotated with main chain of B oriented normal to MMT surface. All binding energy are favorable (i.e., negative values), indicating an overall thermodynamic compatibility among all system components, as expected.

Table 1: Binary binding energy (kcal/mol) and basal spacing (Å) with cloisite 20A® and MMT for homopolymers AN, S, B and block copolymer SAN and polyB-SAN/a.

Polymer	$E_{MMT\text{-}pol}$ [kcal/mol]	$E_{MMT\text{-}quat}$ [kcal/mol]	$E_{pol\text{-}quat}$ [kcal/mol]	Basal spacing [nm]
PS	-24	-1216	-32	
PB	-7	-1266	-16	
PAN	-41	-1248	-100	
SAN	-9	--1165	-36	3.108
ANS	-15	-1102	-146	
polyB-SAN	-5	-1386	-116	
polyB-SANa	-19	-1230	-71	

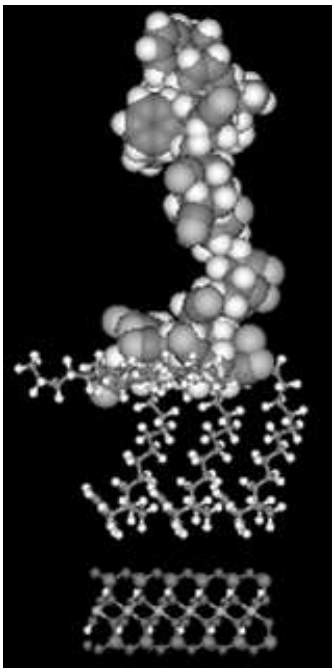

Figure 2: 3D periodic system of a ternary (MMT-quat-polymer) system.

By looking at the values of the $E_{pol\text{-}quat}$ term in Table 1, is evident that the most polar AN homopolymer is more affine to quat than all other ABS homopolymer chain components. In an analogous way, B homopolymer binding energies are smaller. Finally, if one considers the mean binding energy of SAN and ANS (91.0 kcal/mol) and the binding energy for AN, the corresponding values are, respectively, very similar. The same can be noticed if one compares the mean values of the binding energy for polyB-SAN (93.5 kcal/mol), and SAN or AN. This can be sensibly explained with a minor contribution afforded to the total binding energy by the S and B blocks. This last consideration ultimately allow us to consider the smaller, rigid and less ramified SAN block copolymer into MMT layers, as the most probable mode of insertion.
This assumption will be later confirmed by ABS mesoscale modeling and by literature data (Stretz et al. 2005): rubbery phase (polyB-SAN) seems to segregate, forming round islands. This can be also seen in Figure 3, a 3D mesoscale volumetric visualisation.

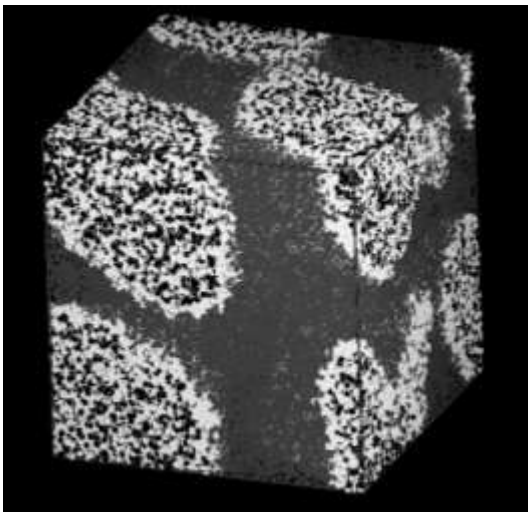

Figure 3: ABS mesoscale simulation. PolyB-SAN tends to form black-and-white islands.

Once again, binding energies and literature data (Stretz et.al., 2005) confirm that these nanocomposites have the same structure, where only SAN partially exfoliates MMT layers, and polyB-SAN creates islands outside the stacks, surrounded by a SAN bulk phase. In Figure 4, a scheme of our 2-phases FEM Palmyra simulations is presented: the MMT stack with SAN intercalation (where overall Young's modulus has been calculated with the 1st Palmyra simulation), and the whole system with MMT stacks and rubbery phases. Polymer bulk properties have been obtained from previous simulations.

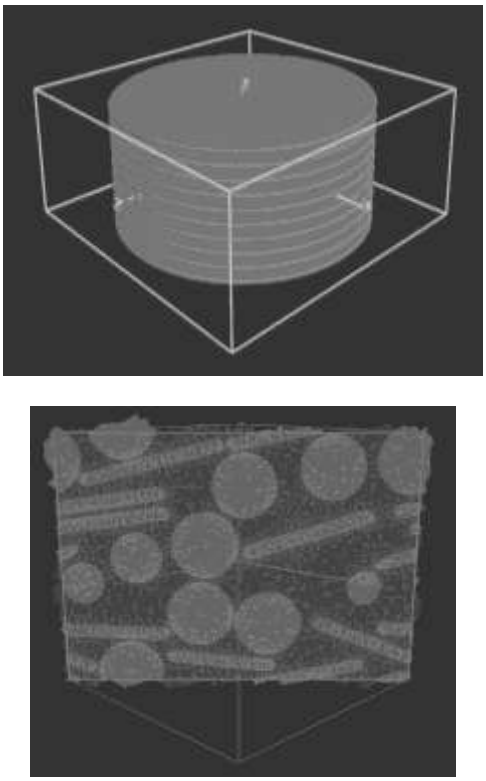

Figure 4: 3D cell visualizations of Palmyra simulations, (up) MMT stack with SAN, (down) whole system.

Table 2 shows overall results for ABS and nanocomposite Young's modulus predicted by Palmyra. The small discrepancy between the experimental and the calculated data is due to the slightly different formulation of ABS used in the calculation, as ABS has a wide range of compositions. For this reason, a comparison of G/G_0 ratio (ratio of nanocomposite and pure ABS Young's modulus) between simulations and experiments were also done.

Table 2: Young's modulus for ABS-MMT nanocomposite and comparison with Stretz et.al, 2005.

Overall properties	% MMT	Calculated	Experimental
G_0 [GPa]	0	2.42	2.20
G [GPa]	2	3.15	2.75
G/G_0	2	1.30	1.25

Polyamide based system. In this case, atomistic simulation allowed us to calculate binding energies between the different beads that we defined in order to fit the particular structure (polymer intercalated clay) we wanted to simulate. Despite the other system, we used mesoscale simulation to model the space between two

intercalated clay layers and subsequently imported the resulting density fields in Palmyra (see Figure 7), in order to calculate mechanical and barrier properties for small stacks of intercalated particles. This clearly constitute a different method with respect to the one discussed for ABS PCN. Finally, models of the whole PCN (a box containing 36 single layer and stack clay particles, see Figure 8) have been modeled with Palmyra using different degrees of exfoliation and different stack dimensions and properties, according to literature data (Esfand et al. 2001 and Duncan et al 2005) and DPD box analysis, respectively.
In this study, the interactions parameters needed as input for the mesoscale level DPD calculations have been obtained by a mapping procedure of the binding energies values between different species obtained from simulations at the atomistic scale, using a simple combinatorial procedure described in details in our previous paper (Scocchi et al. 2007).

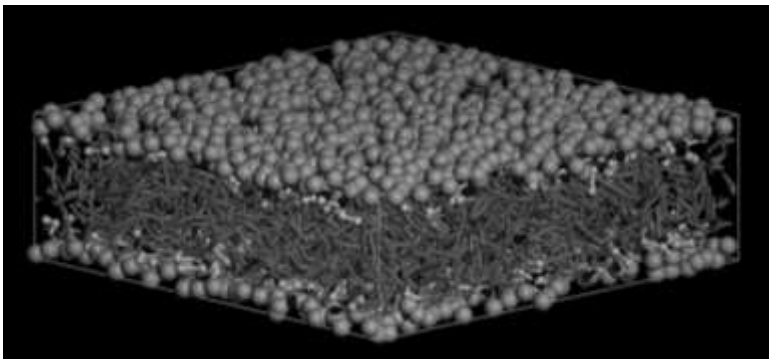

Figure 7: Morphology of the PCN system made up by a MMT platelet, Nylon6, and M_3C_{18} quat molecules obtained via DPD simulation.

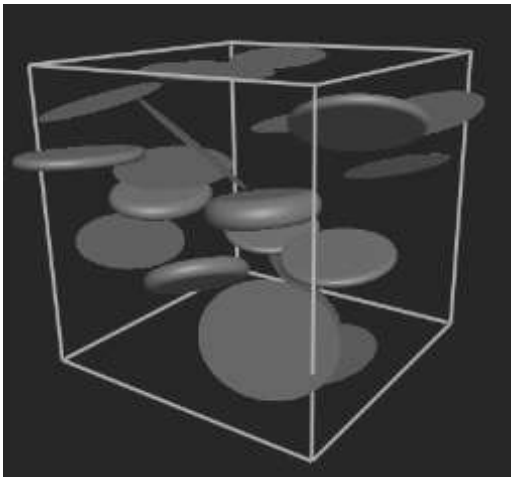

Figure 8: Morphology of the PCN system made up by a MMT platelet, Nylon6, and M_3C_{18} quat molecules obtained with Palmyra. Single platelets are in brown, stacks in red.

Calculations of the Young modulus yielded results which are comparable to experimental data if we consider the values along the *x* e *y* directions (i.e., parallel to the simulated extrusion direction). Eventual discrepancies between virtual and experimental data could be due, for instance, to a different degree of crystallinity or different crystalline forms of Nylon6 in presence of MMT nanofillers, as claimed by some authors (Malik et al 2000 and Fraaije 1993). All estimated values for the nanocomposite with M_3C_{18} as quat are higher than the corresponding ones relative to the PCN with $M_2(C_{18})_2$, in harmony with the different degree of exfoliation that has been modeled. As far as permeability is concerned, it is possible to note that, as expected, O_2 diffusion is hindered only in the *z* direction, i.e. perpendicular to platelet $x - y$ plane. Permeability is anyway reduced only to a small extent (approximately 10 – 15%), because of the low nanofillers content (less than 2% in volume). Data are reported in Table 3.

Table 3: Values of the Young modulus *(E)* and O2 permeability *(P)* in the *x*, *y*, and *z* directions for the 36 particles boxes of both PCNs considered.

36 particle box for PCN with $M_2(C_{18})_2$					
E_{xx}	E_{yy}	E_{zzx}	P_{xx}	P_{yy}	P_{zz}
[GPa]	[GPa]	[GPa]	[barrer]	[barrer]	[barrer]
3.85×10^{2}	3.76×10^{2}	3.20×10^{0}	1.52×10^{-2}	1.52×10^{-2}	1.37×10^{-2}
36 particle box for PCN with M_3C_{18}					
E_{xx}	E_{yy}	E_{zzx}	P_{xx}	P_{yy}	P_{zz}
[GPa]	[GPa]	[GPa]	[barrer]	[barrer]	[barrer]
4.04×10^{2}	4.03×10^{2}	3.23×10^{0}	1.52×10^{-2}	$1.54\times10_{-2}$	1.34×10^{-2}

4. CONCLUSION

In this work we showed how multiscale simulations may be helpful to investigate practical problems in material science, with the main goal of reducing time and costs of experimental analysis. Flexible procedures developed in this work have been validated against various experimental data, confirming their potentialities in material design and property predictions. In this way, we developed new, useful tools for the understanding of structure, phase morphologies and mechanical properties of complex polymer-based nanocomposite system. Moreover, have define criteria leading to the correct choice of the best components for PCNs, and predict macroscopic properties improvements upon material nano engineerization.

5. REFERENCES

Altevogt P., Evers O.A., Fraaije J.G.E.M, Maurits N.M., van Vlimmeren B.A.C. (1999). *J. Mol. Struct. (Theochem)*, 463, 139.

Bicerano J. (2002). Prediction of Polymer Properties, Third Edition, *Marcel Dekker Inc.*, New York

Charpentier J. C. (2002). *Chemical Engineering Science*., 57, 4667

Cosoli P., Scocchi G., Pricl S., Fermeglia M. (2007). *Micro & Meso Materials*., in press

Duncan R., Izzo L. (2005). *Adv. Drug. Delivery Rev.*, 57, 2215

Esfand R., Tomalia D. A. (2001). *Drug Discovery Today*, 6, 427

Fermeglia M., Cosoli P., Ferrone M., Piccarolo S., Mensitieri G., Pricl S. (2006). *Polymer*, 47, 5979.

Fermeglia M., Ferrone M., Pricl S. (2003). *Fluid Phase Equilibria*, 212, 315.

Flory P. J. (1974). Principles of polymer chemistry, *Cornell University Press*, Ithaca.

Fraaije J. G. E. M. (1993). *J. Chem. Phys.*, 99, 9202.

Gusev A., (1997). *J. Mech. Phys. Solids*, 45, 1449.

Hoogerbruge P. J., Koelman J. M. V.A. (1992). *Europhys. Lett.*, 18, 155.

Koelman J. M. V.A., Hoogerbruge P. J. (1993). *Europhys. Lett.*, 21, 363.

Malik N., Wiwattanapatapee R., Klopsch R., Lorenz K., Frey H., Weener J.W., Meijer E.W., Paulus W., Duncan R. (2000). *J. Control. Release*, 65, 133

Mattice W.L., Suter U.W. (1994). Conformational theory of large molecules: the rotational isomeric state model in macromolecular systems, Wiley, New York

Scocchi G., Posocco P., Danani A., Pricl S., Fermeglia M. (2007). *Fluid Phase Eq*., 261, 366

Scocchi G., Posocco P., Fermeglia M., Pricl S. (2007). *J. Phys. Chem. B*, 111, 2143

Stretz H.A., Paul D.R., Cassidy P.E. (2005). *Polymer*, 46, 3818.

Tanaka G., Goettler L. A. (2002). *Polymer*, 43, 541.

Toth R., Coslanich A., Ferrone M., Fermeglia M., Pricl S., Miertus S., Chiellini E. (2004). *Polymer*, 45, 8075

Utracki L.A. (2004). Clay-Containing Polymer Nanocomposites, Rapra Technology Ltd, Shawbury, UK.